Scientia Iranica C (2022) 29(6), 3119–3131

Sharif University of Technology
Scientia Iranica
Transactions C: Chemistry and Chemical Engineering
http://scientiairanica.sharif.edu

Enhancement of electrical conductivity of bismuth oxide/activated carbon composite

Y. Astuti[a,*], R. Mei[a], A. Darmawan[a], Arnelli[a], and H. Widiyandari[b]

a. *Chemistry Department, Faculty of Sciences and Mathematics, Universitas Diponegoro. Jl. Prof. Soedharto, S.H. Tembalang Semarang, Central Java 50275, Indonesia.*
b. *Department of Physics, Faculty of Mathematics and Natural Science, Universitas Sebelas Maret, Jl. Ir. Sutami 36 A, Surakarta, Central Java 57126, Indonesia.*

Received 1 March 2021; received in revised form 26 September 2021; accepted 14 February 2022

KEYWORDS
Activated carbon rice husk;
Bismuth oxide;
Composite;
Hydrothermal;
Battery anode.

Abstract. This study aims to synthesize bismuth oxide/activated carbon composites composed of rice husks for battery anodes and to determine the effect of bismuth nitrate pentahydrate mole variations on the characteristics of the resulting composites. The bismuth oxide/activated carbon composite synthesis was carried out using bismuth nitrate pentahydrate, sodium sulfate, and sodium hydroxide precursors, which were mixed with rice husk-based activated carbon. A variation was made for the mole of bismuth nitrate pentahydrate used, while the compositions of activated carbon and other precursors were made fixed. The composites were synthesized via the hydrothermal method at a temperature of 110°C for 5 hours. The results illustrate that bismuth oxide is successfully formed as a composite in the 8 mmol variation with a composite electrical conductivity value of 2.40×10^{-3} S.m^{-1}.

1. Introduction

Batteries are considered the most effective and practical technology to supply power to electronic devices due to their flexible design and long usage time. Battery performs as a result of oxidation-reduction electrochemical reactions in the battery cells, i.e., transfer of conductive electrons from the negative electrode (anode) to the positive electrode (cathode), to produce electricity and a potential difference.

One indicator for the functionality of a battery is the electrochemical cycling performance which is dependent on the anode materials that the battery comprises. Yao and Cojocaru reported that materials with a large energy capacity and a flexible structure would allow for the repeated insertion and release of lithium ions to carry off a long life cycle [1]. In addition, good anode material must have characteristics, e.g., good charge/ion conductivity ($> 10^3$ Sm^{-1}), high coulomb output (Ahg^{-1}), good efficiency as a reducing agent, good electrical conductivity, stability, easy manufacturing process, and low cost [2].

One material that can be used as an anode material with a large specific capacity is bismuth oxide [3–7]. Li et al. [8] reported that bismuth oxide (Bi_2O_3) had a fairly high volumetric capacity of around 3765 mAhcm^{-3}, good electrical and optical properties with a bandgap of 2.8 eV, and a potential difference of 1.75–2.25 V, and non-toxicity. In addition, bismuth

*. *Corresponding author. Tel.: +62 8567350285; Fax: +62(024) 76480690*
E-mail addresses: yayuk.astuti@live.undip.ac.id (Y. Astuti); roshanameifajarwati@gmail.com (R. Mei); adi.darmawan@live.undip.ac.id (A. Darmawan); arnelli@live.undip.ac.id (Arnelli); hendriwidiyandari@staff.uns.ac.id (H. Widiyandari)

doi: 10.24200/sci.2022.57674.5359

is environmentally-friendly and relatively low in price compared to noble metals [9,10]. Based on these advantages, Bi_2O_3 is considered a promising anode material for lithium-ion batteries with high energy density [11,12]. However, the problem with using bismuth oxide as an anode is that it has a low electrical conductivity value. This, nonetheless, can be overcome by combining other materials characterized by better electrical conductivity values, one of which is activated carbon from rice husks.

Rice husk-based activated carbon has been widely studied and utilized for energy applications [13]. Yu et al. [14] reported that the electrochemical performance of rice husk-based activated carbon significantly improved in comparison to that of the non-activated carbon. In addition, Wang et al. found that the activated carbon from rice husks had an electrical conductivity value of as high as 21.6 Sm^{-1} [15] as well as a large surface area of 300 m^2g^{-1} to 3500 m^2g^{-1} [16]. Activated carbon had a volumetric capacity of 1770 $mAhcm^{-3}$ and a potential difference of 0.2 V [17], which could be expected to increase the electrical conductivity of bismuth oxide as a battery anode. It was reported that the combination of a metal or metal oxide with carbon had a great impact on the dynamic diffusion of ions and the performance of electrochemical properties [18–20]. For example, carbon-coated Bi_2O_3 nanocomposite (Bi_2O_3@C) prepared by redox reaction was applied as anode material for Sodium Ion Battery (SIB) [21]. This Bi_2O_3@C nanocomposite exhibited excellent cycle stability after 100 cycles with a discharge capacity of 421 $mAhg^{-1}$ at a current density of 1500 mAg^{-1} [7]. Carbon can be used as a conductive support and it forms an active ingredient to prevent particle agglomeration [22]. Carbon acts as a framework to retain volume changes, increase electrical conductivity, and prevent particle agglomeration in Li ions extraction/intercalation [23]. When the particles (bismuth oxide) are agglomerated, the particles are not well distributed such that the diffusion of Li ions is disrupted and the elimination of electrical connectivity among particles is facilitated, thereby blocking the access of Li ions to active particles [24].

Furthermore, synthesis of bismuth oxide/carbon composites as anode material has been undertaken previously. Demir et al. [7] reported that the bismuth oxide nanoparticles incorporated into carbon nanofiber produced from organic compounds exhibited excellent capability and superior capacities in sodium ion batteries. Moreover, self-standing Bi_2O_3 nanoparticles/carbon nanofiber hybrid films were successfully produced as a binder-free anode for sodium batteries [5]. Aprialdi et al. [25] found that the synthesis and characterization of bismuth oxide/activated carbon composites for battery anodes using the hydrothermal method with variations in the weight ratios of activated carbon to bismuth nitrate pentahydrate at 2:1, 1:1, and 1:2 resulted in the electrical conductivity of each variation of 0.59×10^{-5} Sm^{-1}, 1.24×10^{-5} Sm^{-1}, and 0.51×10^{-5} Sm^{-1}, respectively. However, X-Ray Diffraction (XRD) results illustrated that bismuth oxide was not fully formed in the composite, and Scanning Electron Microscope (SEM) findings demonstrated that the distribution of carbon was more dominant than bismuth [25].

Based on this background, it is apparent that a bismuth oxide/activated carbon composite is fabricated using a more precise composition and method. In the present study, the bismuth oxide/activated carbon composite was synthesized by the hydrothermal method. The hydrothermal method was chosen because of the relatively low-temperature use, safe reaction process, non-requirement for reducing agents [26], and higher homogeneity and purity of the resulting material [27]. More importantly, it is reported that bismuth oxide with higher electrical conductivity values is successfully formed [28]. The combination of rice husk activated carbon with bismuth oxide is expected to generate improved electrical conductivity in the resulting composite.

2. Method

2.1. Materials

The materials used in this study were crystals of $Bi(NO_3)_3.5H_2O$ (Sigma Aldrich), distilled water, H_3PO_4 60% (v/v), Na_2SO_4 powder, and NaOH crystals (Merck), and activated carbon (CA) provided from rice husks.

2.2. Procedures

2.2.1. Synthesis of rice husk-based activated carbon

The making of rice husk activated carbon was carried out through the carbonization and activation stages. At the carbonization stage, cleaned rice husks were charred through pyrolysis at a temperature of 300°C for 10 minutes. A total of 5 grams of the carbon product from the pyrolysis was then activated with 125 mL H_3PO_4 60% (v/v) and heated in a microwave with 400 watts of power for 5 minutes. The activated carbon was then washed with distilled water until the pH would become constant. The activated carbon that had been washed was then dried using an oven at 105°C for 1 hour. The produced activated carbon was then crushed and sieved with a mesh size of 100 [29].

2.2.2. Synthesis of bismuth oxide/activated carbon composite

A total of 8 mmol of $Bi(NO_3)_3.5H_2O$ was added with 12 mmol of Na_2SO_4, dissolved in 40 mL of distilled water, and stirred using a magnetic stirrer (IKA RH Basic KT/C) at 1500 rpm for 45 minutes. The mixture was then added 40 ml of 72 mmol of NaOH [27]. The

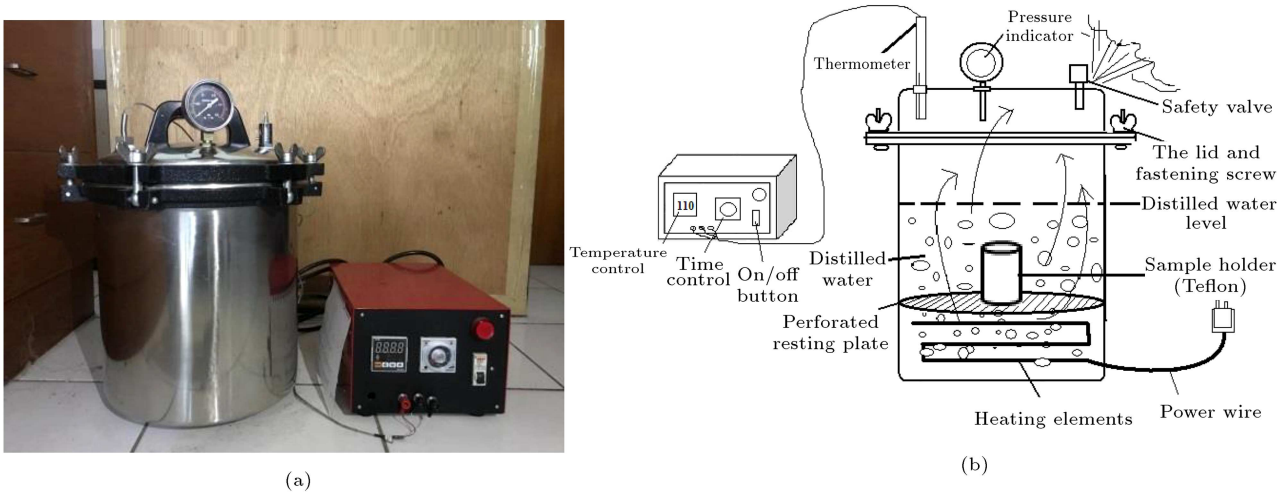

(a) (b)

Figure 1. (a) Hydrothermal reactor and (b) reactor scheme.

next step was the addition of 0.5 grams of activated carbon rice husk to the mixture. The mixture was then fed to a hydrothermal reactor (Figure 1) and heated at 110°C for 5 hours. The resulting mixture was cooled and then, filtered. The filtered precipitate was dried using an oven (fisher scientific) at 110°C for 60 minutes. After that, it was sieved with the mesh size of 100. The same procedure was applied to manufacturing bismuth oxide/activated carbon composites with 24 mmol and 32 mmol variations.

2.2.3. Characterization of bismuth oxide/activated carbon composite

The resulting bismuth oxide/activated carbon composite material was characterized by Fourier Transform Infra-Red (FTIR) (Shimadzu IRAffinity-1) analysis to determine the functional groups of the composite materials carried out at wavenumbers 4000 to 400 cm^{-1} at a frequency rate of 0.25 cm^{-1} at room temperature. Products were also analyzed using XRD (Shimadzu 7000) to identify the crystal structures. Measurements were conducted for 2θ with Cu-Kα radiation (λ = 0.15406 nm). The surface morphology and distribution of bismuth oxide and activated carbon in the composites were characterized using SEM Jeol JED 6510LA with magnifications of 100× and 5000×, supported by mapping and elemental analysis using Energy Dispersive X-ray (EDX). Characterization using TGA-DTG with Mettler Toledo TGA/DSC 3+ was done to determine the thermal stability of composite materials. The sample analysis was carried out in the temperature range of 40–800°C at a heating rate of 4°C/m in a nitrogen atmosphere. Characterization of the composites using Gas Sorption Analyzer (GSA) (Tristar II 3020) was done to determine pore size and pore distribution. The samples were analyzed using nitrogen gas flow (N_2). Finally, the products were characterized using the HIOKI 3532-50 LCR meter to determine the electrical conductivity values of the composites. The samples were prepped as pellets with a diameter of 1.5 cm and a thickness of 2–5 mm for the analysis.

3. Results and discussion

3.1. Activated carbon

Activated carbon synthesis was carried out according to the procedure reported by Santoso [29]. The process was carried out in two stages, namely the pyrolysis of rice husks to carbon and the carbon activation using H_3PO_4 acid. The pyrolysis process of rice husks produced carbon, tar, and permanent gases such as CO_2, CO, CH_2, H_2, and others [30]. The product of this carbonization was blackened carbon.

The pyrolyzed carbon was activated using phosphoric acid by heating it using microwave radiation. The activation process aimed to enlarge and open carbon pores and increase the surface area of the carbon. Phosphoric acid can remove impurities contained in carbon from the carbonization process (rice husks) such as ketones, alcohol, acids, and aldehydes [31,32]. The activated carbon sample obtained was a fine black powder with uniform size. The synthesis scheme of the activated carbon from rice husks is seen in Figure 2.

3.2. Bismuth oxide/activated carbon composites

The synthesis of bismuth oxide/activated carbon composites with mole variation in the used bismuth nitrate pentahydrate was initiated via the reaction of $Bi(NO_3)_3.5H_2O$, Na_2SO_4, and NaOH precursors. The solution was later added with rice husk activated carbon, homogenized, and heated in a hydrothermal reactor. The reaction mechanism for the formation of bismuth oxide according to Wu et al. [27] is given below:

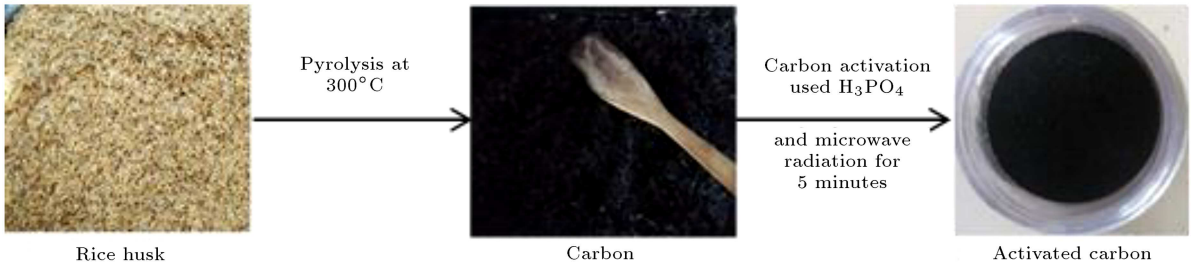

Figure 2. Activated carbon synthesis scheme.

Figure 3. Bi/CA synthesized composites using (a) 8 mmol, (b) 24 mmol, and (c) 32 mmol bismuth nitrate pentahydrate.

$$2Bi(NO_3)_3.5H_2O + Na_2SO_4 \rightarrow Bi_2\ O(OH)_2SO_4 + 2NaNO_3 + 4HNO_3 + 7H_2O, \quad (1)$$

$$Bi_2(OH)_2SO_4 + 2NaOH + H_2O \rightarrow 2Bi(OH)_3 + Na_2SO_4, \quad (2)$$

$$2Bi(OH)_3 \rightarrow Bi_2O_3 + 3H_2O. \quad (3)$$

The resulting composite from the 8 mmol variation was blackish gray powder with a smooth dark gray texture. At 24 mmol variation, the resulting composite was light gray fine powder; at 32 mmol variation, the resulting composite was gray-colored ash with a texture resembling an agglomerate, as shown in Figure 3. The gray color was produced from the combination of pale yellow from the bismuth oxide and black from the activated carbon.

3.3. Characteristics of bismuth/oxide composites

3.3.1. Structure

Figure 4 shows the FTIR spectra of activated carbon, pure bismuth oxide, and the composites made in this study. The rice husk activated carbon had a small rate of absorption at a wavenumber of about 3400 cm^{-1} denoting the absorption of the OH group, 1642 cm^{-1}

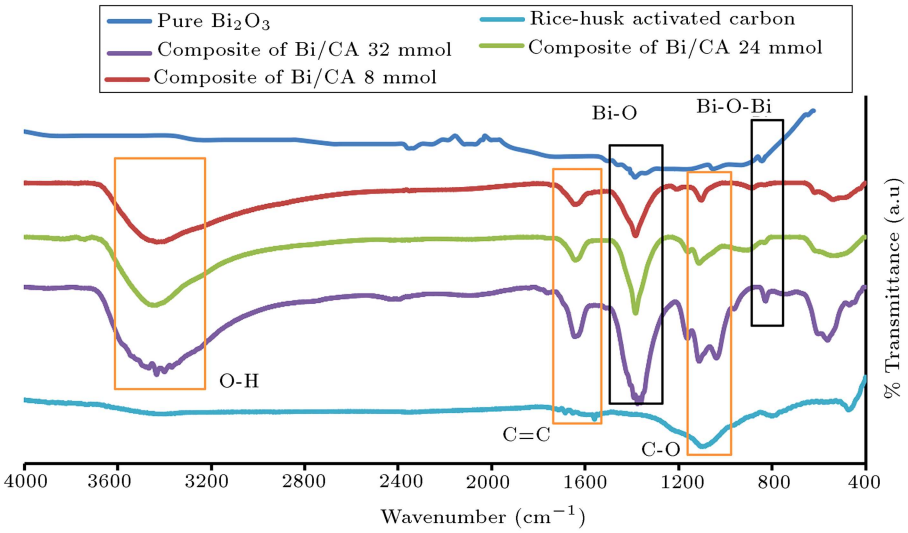

Figure 4. FTIR spectra of pure bismuth oxide [37], rice husk activated carbon [29], and the bismuth oxide/activated carbon composite samples.

referring to the C=C group, and 1095 cm^{-1} indicating the presence of a CO group [33,34].

Similar absorption was exhibited by each of the composite samples, namely the C=C group in the absorption area around 1642–1645 cm^{-1} and the C-O group seen in the absorption area around 1100 cm^{-1}. Meanwhile, the pure bismuth oxide spectra present the Bi-O-Bi group absorption peak in the 829 cm^{-1} area [35–37] and the Bi-O group at a wavenumber of about 1380 cm^{-1} [38].

The three samples of bismuth oxide/activated carbon composites have almost the same spectra as the two raw materials combine, showing the presence of a fairly sharp peak in the area of around 828–830 cm^{-1} indicating the Bi-O-Bi group and in the area of 1375–1384 cm^{-1} indicating the Bi-O group. Thus, it can be concluded that bismuth oxide was successfully formed in each of the composite samples. Additionally, the three composite samples were also observed to have a wide O-H absorption at the wavenumber of about 3400 cm^{-1}.

Complete data regarding the functional groups of bismuth oxide/activated carbon composites, bismuth oxide (Bi_2O_3), and rice husk activated carbon from the FTIR test results are shown in Table 1.

3.3.2. Crystal structure

XRD results, as presented in Figure 5, show that the diffractogram of the 8 mmol Bi/CA composite sample substantially matched the α-Bi_2O_3 diffractogram while slightly matching the β- and γ-Bi_2O_3 diffractogram. The 8 mmol Bi/CA composite had high peak values at 2 theta (2θ) of 27.430°, 33.090°, 33.296°, and 46.246°. The 2 theta (2θ) values were almost the same as the α-Bi_2O_3 peak values at 27.377°, 33.039°, 46.305° with miller indices (120), (121), (200), and

Table 1. Functional groups observed in the samples.

Functional groups	Sample wavenumbers (cm^{-1})				
	Activated carbon	Bismuth oxide	Bi/CA 8 mmol	Bi/CA 24 mmol	Bi/CA 32 mmol
-OH	3400	—	3432.84	3436.72	3433.46
Bi-O	—	1384	1384.14	1384.02	1375.91
Bi-O-Bi	—	829	830.88	829.22	828.44
C=C	1642	—	1644.41	1642.49	1644.95
C-O	1095	—	1103.13	1112.25	1111.85

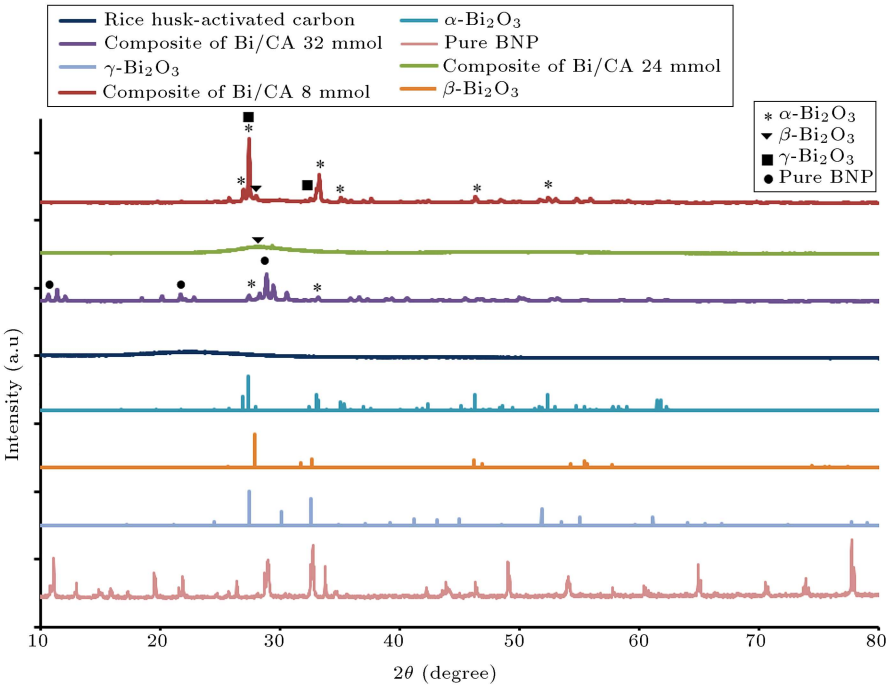

Figure 5. Diffractogram of composites (Bi/CA 8 mmol, 24 mmol, and 32 mmol), pure bismuth nitrate pentahydrate, rice-husk activated carbon, data base α-Bi_2O_3 (JCPDF No. 41-1449), β-Bi_2O_3 (JCPDF No. 76-0147), and γ-Bi_2O_3 (JCPDF No. 45-1344).

(041), respectively, based on JCPDF No. 41-1449. This is a strong suggestion that the Bi/CA 8 mmol composite contained bismuth oxide crystals with α-Bi_2O_3 (monoclinic) structure being more dominant than β-Bi_2O_3 and γ-Bi_2O_3 in which β-Bi_2O_3 peak value is determined at 2 theta (2θ) 27.799 with miller index (201) (JCPDF No. 76-0147), while the presence of γ-Bi_2O_3 is indicated by (2θ) values at 27.455° and 32.607° with miller indices (310) and (321), respectively (JCPDF No. 45-1344).

Furthermore, the 24 mmol Bi/CA composite diffractogram showed that the composite had a non-crystalline (amorphous) structure. This indicates that the Bi/CA 24 mmol composite did not bear bismuth oxide. The diffractogram of the 32 mmol composite had its highest peaks at 2 theta (2θ) of 28.900°, 29.473°, and 30.592° with the miller indices ($01\bar{2}$), ($1\bar{3}0$), (012) based on JCPDF No. 44-0314, showing no compatibility with α-β- and γ-Bi_2O_3 diffractograms, but merely a match with the diffractogram peaks of bismuth nitrate pentahydrate. These peaks are also considered as the peaks of the by-product $Bi_2O(OH)_2SO_4$ [27] formed during the reaction (reaction 1). However, the 32 mmol Bi/CA composite diffractogram had small peaks at 27.421° and 33.209° with miller indices (120) and (200), respectively, which indicated a good match with α-Bi_2O_3. This implies that the 32 mmol Bi/CA composite contained more bismuth nitrate pentahydrate precursor and $Bi_2O(OH)_2SO_4$ by-product than bismuth oxide. Qualitatively, the 32 mmol Bi/CA composite diffractogram had several discrete peaks, indicating that the 32 mmol composite had a crystalline structure. Meanwhile, the diffractogram of activated carbon shows that this material has an amorphous structure. This finding is in accordance with the research reported by Wazir et al. [39].

3.3.3. Morphology and particle distribution of bismuth oxide

SEM images of bismuth oxide/activated carbon composites with 8 mmol, 24 mmol, and 32 mmol variations are shown in Figure 6. Figure 6 shows that the 8 mmol variation of the Bi/CA composites had a rod-like particle shape with a length of 5.14–19.16 μm and a width of 0.83–1.66 μm. The rod-like particle shape marked the presence of bismuth oxide in the composite, which is in agreement with the study reported by Wu et al. [27]. Meanwhile, the Bi/CA composite with 24 mmol variation was characterized by irregular particle-shape, cluster-like clouds. Furthermore, the Bi/CA composite with 32 mmol variation illustrated that the particles had irregular shapes and formed agglomerations with particle sizes of about 1.35–3.37 μm. This sample also appeared to have a less hollow or porous surface which was theorized to originate from the pores that were covered by the dominant elements in the composite. The SEM mapping images of the three composite samples are shown in Figure 7.

Figure 7 illustrates the distribution of the bismuth (Bi), carbon (C), oxygen (O), and Si elements in the Bi/CA composites in the 8 mmol, 24 mmol, and 32 mmol variations, respectively, marked by red, green, yellowish-green, and blue, respectively. Figure 7 shows that the 8 mmol variation of the composites had Bi and C elements that appeared almost balanced and evenly distributed across the surface of the material. In the 24 mmol variation, it can be seen that the material surface was more dominated by the distribution of Bi elements, whereas at the 32 mmol variation, the distribution of Bi and O elements dominated the sample surface and caused the C element to be less visible on the sample surface.

3.3.4. Thermal stability of composites

TGA-DTG characterization was employed to determine the decomposition process and thermal stability of the composite materials. The TGA-DTG characterization results of each mole variation of bismuth nitrate pentahydrate are shown in Figure 8.

Based on the results of the TGA and DTG analyses in Figure 8, the 8 mmol and 24 mmol samples exhibit five stages of the decomposition process, while the 32 mmol sample has four stages of decomposition. In Stage I, decomposition occurred in the temperature

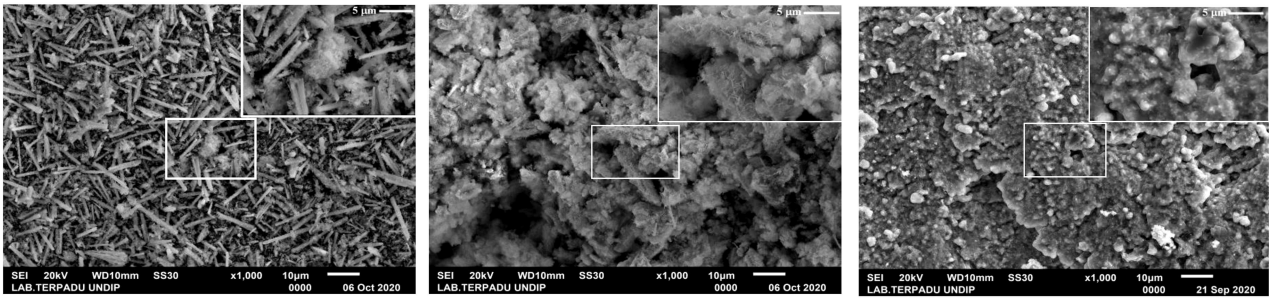

(a) (b) (c)

Figure 6. SEM images of Bi/CA composites synthesized using (a) 8 mmol, (b) 24 mmol, and (c) 32 mmol bismuth nitrate pentahydrate.

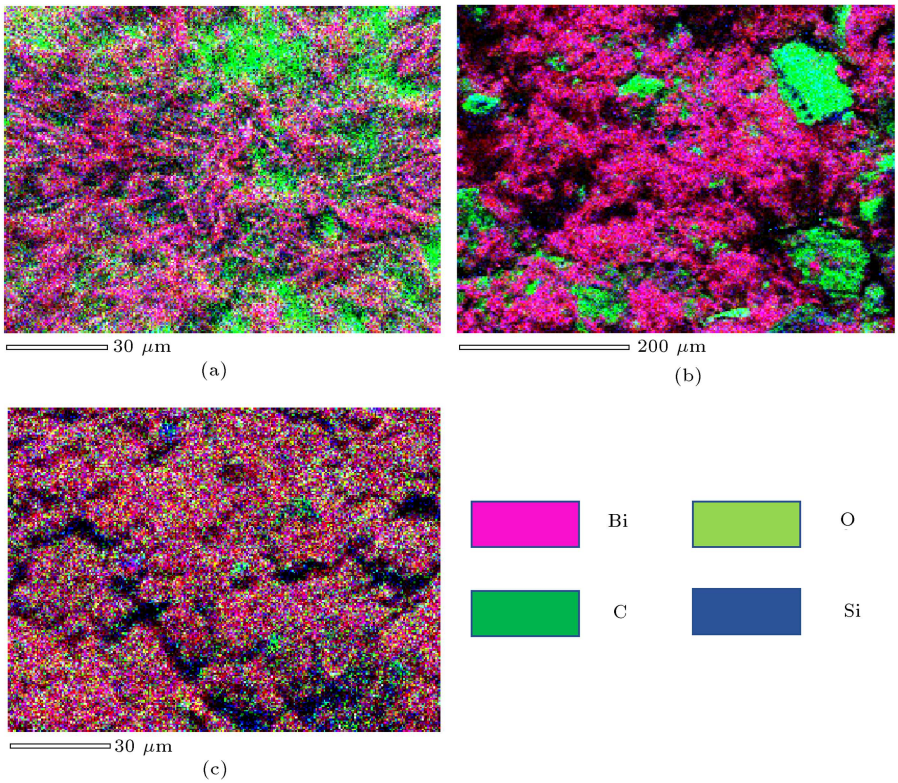

Figure 7. SEM mapping of Bi/CA composites synthesized using (a) 8 mmol, (b) 24 mmol, and (c) 32 mmol bismuth nitrate pentahydrates.

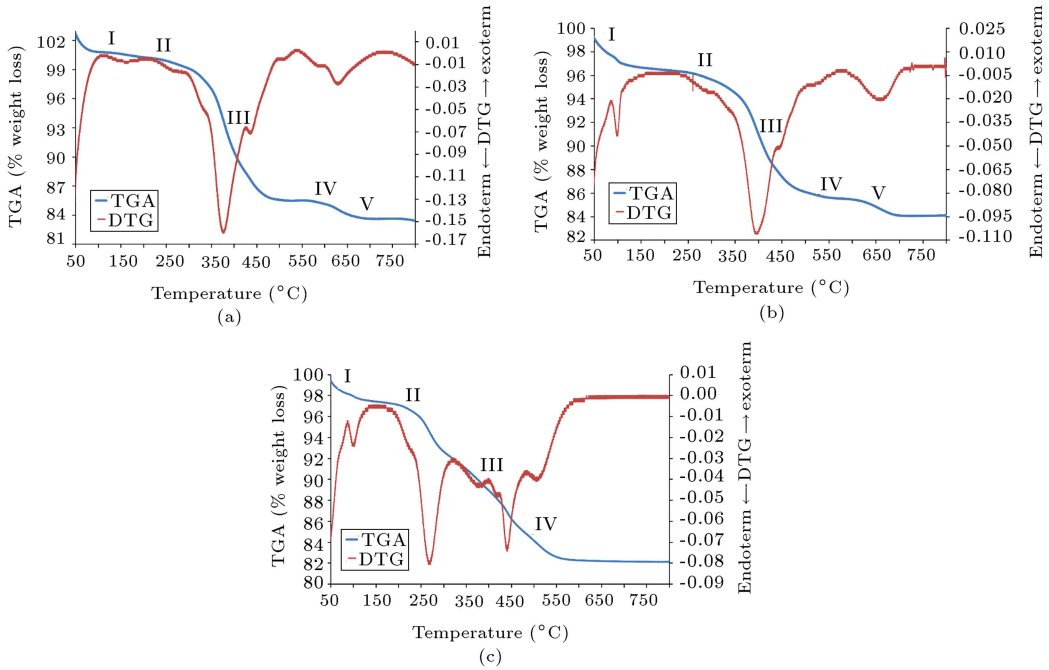

Figure 8. Thermal stability of composites analyzed using TGA-DTG.

range of 75°–190°C, indicating the evaporation of water content adsorbed onto the surface of the activated carbon [34]. The weight loss at this stage also indicates the rapid evaporation of organic volatiles under an oxygen atmosphere [40].

Stage II took place in the temperature range of 225°–320°C, which was assumed to be the burning process of cellulose and hemicellulose which were present in the activated carbon [40], in addition to the removal of residues [41] such as $NaNO_3$, NaOH, and SO_4^{2-}.

The weight reduction for Stage II of the 32 mmol variation was larger than the weight loss graph for Stage II for the 8 and 24 mmol variations. This result indicated that more residues were decomposed at the 32 mmol variation as it contained the reaction byproduct, $Bi_2O(OH)_2SO_4$, and the $Bi(NO_3)_3.5H_2O$ precursor as suggested by the XRD results shown in Figure 5.

Stage III occurred in the temperature range of 330°–500°C, showing a significant reduction in weight for each composite. The weight of the 8 mmol variation sample was lost from 94.86% to 81.51%, amounting to the weight loss of around 13.35%. The 24 mmol variation experienced a weight loss percentage of about 8.42%, whilst the 32 mmol variation showed a significant reduction in weight from 91.98% to 85.29%, equating to 6.69%. The weight loss at this stage was interpreted as the phase transformation from the precursor material to bismuth oxide [41], which occurred endothermically.

Stage IV of decomposition occurred in the range of 500°–610°C, indicating the formation of monoclinic alpha bismuth oxide (α-Bi_2O_3) and the transformation from the monoclinic structure to the body-centered cubic (γ-Bi_2O_3) structure [42]. Lastly, Stage V occurred in the range of 640°–700°C denoting the transformation of γ-Bi_2O_3 to α-Bi_2O_3 as the thermal behavior of bismuth oxide is common at temperatures above 600°C [43].

3.3.5. Electrical conductivity

Figure 9 shows the graph of the relationship between the log conductivity and the log frequency of the composites. The x-axis (log frequency) shows the number of electrons flowing to generate electric current, while the y-axis (log conductivity) signifies the sample ability to conduct electric current. The relationship between the two properties is linear, meaning that the higher the frequency, the greater the conductivity. The electrical conductivity value of the sample was determined from the value of the intercept of the graph plateau line equation of each composite sample. The plateau area is an area with stable values of y (log conductivity) (no/very small increase) with respect to the increase in the value of x (log frequency). The conductivity value of the sample was obtained from the antilog of the graph intercept value.

The electrical conductivity values obtained from the Electrochemical Impedance Spectroscopy (EIS) test on the bismuth oxide, rice husk activated carbon (CA), and bismuth oxide/activated carbon (Bi/CA) composite samples with varying bismuth nitrate pentahydrate moles are shown in Table 2.

Based on Table 2, the electrical conductivity value of the rice husk activated carbon was higher than that of pure bismuth oxide. The conductivities of the composites were seen to have increased relative to the pure bismuth oxide and activated carbon.

The electrical conductivity values of the Bi/CA composites from the highest to the lowest were shown by the 32 mmol, 8 mmol, and 24 mmol variations, respectively. The 32 mmol composite sample had a high electrical conductivity value because of the

Table 2. Electrical conductivity of pure bismuth oxide, activated carbon, bismuth nitrate pentahydrate, 8 mmol Bi/CA, 24 mmol Bi/CA, and 32 mmol Bi/CA.

Sample	Electrical conductivity
Pure Bi_2O_3	1.55×10^{-7} S.m^{-1}
Rice husk activated carbon	8.17×10^{-5} S.m^{-1}
Bismuth nitrate pentahydrate	1.70×10^{-1} S.m^{-1}
8 mmol Bi/CA	2.40×10^{-3} S.m^{-1}
24 mmol Bi/CA	4.91×10^{-4} S.m^{-1}
32 mmol Bi/CA	15.54×10^{-3} S.m^{-1}

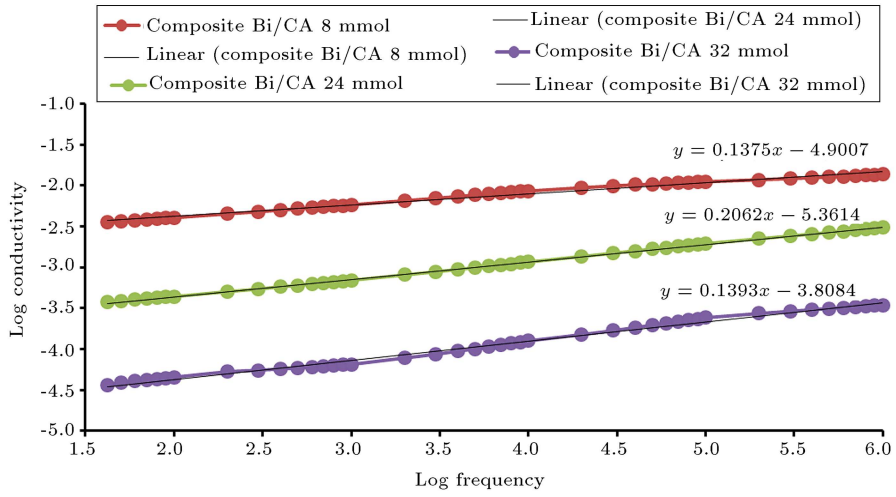

Figure 9. The relationship graph between the log conductivity and the log frequency of the composites.

large amount of bismuth nitrate pentahydrate in the composite, as shown in the XRD results (Figure 5). In addition, the 32 mmol Bi/CA composite exhibited agglomerations that affected the electrical conductivity value, because samples with large crystal sizes have a good level of atomic order that increased the mobility of electrons in the sample [44,45].

The electrical conductivity value of the 8 mmol variation composite was higher than that of the 24 mmol variation. This is because in the 8 mmol Bi/CA composite, neither the precursor material for the formation of bismuth oxide nor the added activated carbon dominated one another. In other terms, the bismuth oxide formed in the composite denoted in the FTIR (Figure 4) and XRD (Figure 5) results were evenly distributed throughout the surface of the material, as seen in the SEM mapping image shown in Figure 7. The even distribution of bismuth oxide would allow for more freedom in the mobility of electrons in the material, thereby increasing the electrical conductivity value [46,47]. The 24 mmol composite had the smallest electrical conductivity value because bismuth oxide had not been successfully formed and its crystal structure was amorphous. Overall, the three composite samples had electrical conductivity values in the range 10^{-8} S.m^{-1} to 10^{-3} S.m^{-1}, indicating that the materials had semiconductor properties [48].

3.3.6. Porosity, pore surface area, and pore size distribution

Characterization of composite samples using a Gas Sorption Analyzer (GSA) aimed to determine the surface area, pore size, pore volume, and pore distribution of the materials. The BET charts of the rice husk were activated and the 8 mmol, 24 mmol, and 32 mmol Bi/AC composites can be seen in Figure 10.

Figure 10 is a graph showing the amount of adsorption and desorption of nitrogen gas (N_2) with respect to relative pressure (p/p_0). The graph shows that the three composite samples had a similar isotherm pattern, namely, type IV isotherm characterized by the hysteresis loop. The hysteresis pattern indicates that the samples are materials that exhibit pores because they could absorb N_2 gas molecules. The GSA results of the rice husk activate carbon and the 8 mmol, 24 mmol, and 32 mmol Bi/AC composites are shown in Table 3.

Table 3 shows that the three composite samples

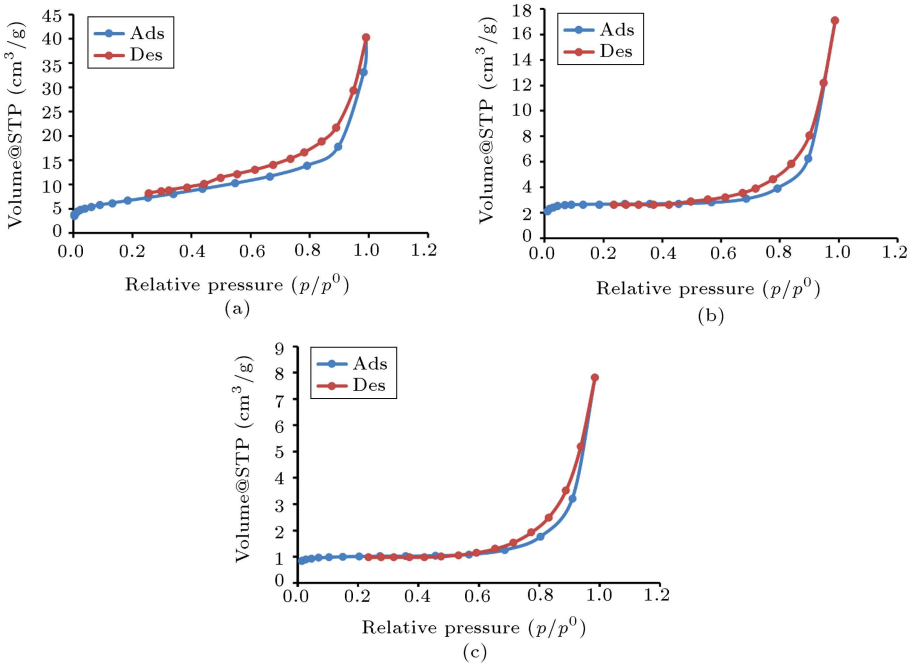

Figure 10. N_2 adsorption/desorption isotherm graphs of (a) 8 mmol, (b) 24 mmol, and (c) 32 mmol Bi/AC composites.

Table 3. Surface area, pore volume, and average pore size.

Sample	S_{BET} (m^2/g)	V_{total} (cm^3/g)	Average pore size (nm)
Rice husk activated carbon	18.837	0.014	3.090
8 mmol Bi/AC composite	24.221	0.051	8.473
24 mmol Bi/AC composite	8.102	0.026	13.055
32 mmol Bi/AC composite	3.113	0.012	15.509

had mesoporous sized pores because the pore radius ranged from 3 to 50 nm [49]. Subhan et al. [50] reported the fabrication and characterization of $Li_4Ti_5O_{12}$ for battery anode materials; porosity would affect the electrical conductivity value of the sample. Samples with high porosity, i.e. those that have many pores with small pore size, will tend to have a low electrical conductivity value because a large number of pores will cause greater resistance, thereby reducing the electrical conductivity of the sample [51,52].

This is in line with the results of the characterization of the 32 mmol Bi/AC composite which demonstrated the largest pore size of 15.509 nm as well as a small pore volume and surface area of 0.012 cm^3/g and 3.110 m^2/g. This depicted that the 32 mmol composite sample had a small number of pores or small porosity, which when analyzed with an LCR meter, the measured resistance was low and the sample electrical conductivity was high, as per the theory mentioned. In addition, material density also affects the electrical conductivity value of the sample. As the density of the material increases, the level of the order of the atoms in the crystal also increases and will consequently increase the value of electron mobility [44,45]. If associated with the characterization results in Table 3, the material density increased in order from the 8 mmol and then 24 mmol to the 32 mmol variations. This can be seen from the value of the total volume of each composite sample which decreased as the number of moles of bismuth nitrate pentahydrate increased. The decrease in pore volume was probably due to the bismuth adsorbed into the pore of the activated carbon. The larger the number of bismuth particles, the more these particles will occupy the activated carbon pores. As a result, the originally large pore volume becomes smaller. Thus, more bismuth could be adsorbed into the pore causing the pore volume to decrease and the material to be clumpy.

4. Conclusion

Befitting compositions in the synthesis of bismuth oxide/activated carbon composites could produce composites with better electrical conductivity values than their precursors. The results showed that bismuth oxide was successfully formed in the 8 mmol variation with an electrical conductivity value of 2.40×10^{-3} $S.m^{-1}$. The highest electrical conductivity value was produced by the variation of 32 mmol, though the bismuth oxide formed was very small based on the X-Ray Diffraction (XRD) results. Its high electrical conductivity value was thought to be derived from the electrical conductivity of bismuth nitrate pentahydrate precursor. This investigation is expected to give recommendation on the use of activated carbon and bismuth oxide in the form of composite as potential candidates for battery anode by paying attention to the factors influencing the formation of composites, especially the composite precursor composition factor. In addition, this investigation is expected to give a scientific contribution.

Acknowledgment

The authors would like to thank the Ministry of Research and Technology/National Research and Innovation Agency of Indonesia for their financial support with the grant number 225-71/UN7.6.1/PP/2020 (Fundamental Research Scheme/Penelitian Dasar) in the fiscal year 2020.

References

1. Yao, F. and Cojocaru, C.S. "Carbon-based nanomaterials as an anode for lithium ion battery", Doctoral Dissertation, Ecole Polytechnique X. (2013).
2. Linden, D. and Reddy, T.B. "Basic concept", In *Handbook of Batteries*, McGraw-Hill, USA, Chapter 1, pp. 19–34 (2002).
3. Nandi, S. and Das, S.K. "An electrochemical study on bismuth oxide (Bi_2O_3) as an electrode material for rechargeable aqueous aluminum-ion battery", *Solid State Ion.*, **347**, p. 115228 (2020).
4. Mei, J., Liao, T., Ayoko, G.A., et al. "Two-dimensional bismuth oxide heterostructured nanosheets for lithium- and sodium-ion storages", *ACS Appl. Mater. Interfaces*, **11**, pp. 28205–28212 (2019).
5. Yin, H., Cao, M.L., Yu, X.X., et al. "Self-standing Bi_2O_3 nanoparticles/carbon nanofiber hybrid films as a binder-free anode for flexible sodium-ion batteries", *Mater. Chem. Front.*, **1**, pp. 1615–1621 (2017).
6. Xiong, T., Xiong, T., Lee, W.S.V., et al. "Bismuth ion battery - A new member in trivalent battery technology", *Energy Stor. Mater.*, **25**, pp. 100–104 (2020).
7. Demir, E., Soytas, S.H., and Demir-Cakan, R. "Bismuth oxide nanoparticles embedded carbon nanofibers as self-standing anode material for Na-ion batteries", *Solid State Ion.*, **342**, p. 115066 (2019).
8. Li, Y., Trujillo, M.A., Fu, E., et al. "Bismuth oxide: a new lithium-ion battery anode", *J. Mater. Chem. A.*, **1**, pp. 12123–12127 (2013).
9. Dai, R., Wang, Y., Da, P., et al. "Indirect growth of mesoporous Bi@C core-shell nanowires for enhanced lithium-ion storage", *Nanoscale*, **6**, pp. 13236–13241 (2014).
10. Huang, Z.-D., Lu, H., Qian, K., et al. "Interfacial engineering enables Bi@C-TiO_x microspheres as superpower and long life anode for lithium-ion batteries", *Nano Energy*, **51**, pp. 137–145 (2018).
11. Hong, W., Ge, P., Jiang, Y., et al. "Yolk-shell-structured bismuth@ N-doped carbon anode for

lithium-ion battery with high volumetric capacity", *ACS Appl. Mater. Interfaces*, **11**, pp. 10829–10840 (2019).

12. Zhong, Y., Li, B., Li, S., et al. "Bi nanoparticles anchored in N-doped porous carbon as anode of high energy density lithium ion battery", *Nanomicro Lett.*, **10**, pp. 1–14 (2018).
13. Wang, Z., Smith, A.T., Wang, W., et al. "Versatile nanostructures from rice husk biomass for energy applications", *Angew. Chem. Int. Ed.*, **57**, pp. 13722–13734 (2018).
14. Yu, K., Li, J., Qi, H., et al. "High-capacity activated carbon anode material for lithium-ion batteries prepared from rice husk by a facile method", *Diam. Relat. Mater.*, **86**, pp. 139–145 (2018).
15. Wang, L., Schnepp, Z., and Titirici, M.M. "Rice husk-derived carbon anodes for lithium ion batteries", *J. Mater. Chem. A*, **1**, pp. 5269–5273 (2013).
16. Jamilatun, S. and Setyawan, M. "Pembuatan arang aktif dari tempurung kelapa dan aplikasinya untuk penjernihan asap cair", *Spektrum Industri*, **12**(1), pp. 73-86 (2014).
17. Kim, T., Jo, C., Lim, W.G., et al. "Facile conversion of activated carbon to battery anode material using microwave graphitization", *Carbon*, **104**, pp. 106–111 (2016).
18. Shrivastav, V., Sundriyal, S., Tiwari, U.K., et al. "Metal-organic framework derived zirconium oxide/carbon composite as an improved supercapacitor electrode", *Energy*, **235**, p. 121351 (2021).
19. Peng, J., Zhang, W., Chen, L., et al. "A versatile route to metal oxide nanoparticles impregnated in carbon matrix for electrochemical energy storage", *Chem. Eng. J.*, **404**, p. 126461 (2021).
20. Wang, R., Li, X., Nie, Z., et al. "Metal/metal oxide nanoparticles-composited porous carbon for high-performance supercapacitors", *J. Energy Storage*, **38**, p. 102479 (2021).
21. Fang, W., Fan, L., Zhang, Y., et al. "Synthesis of carbon coated Bi_2O_3 nanocomposite anode for sodium-ion batteries", *Ceram. Int.*, **43**, pp. 8819–8823 (2017).
22. Ouyang, Y., Chen, Y., Peng, J., et al. "Nickel sulfide/activated carbon nanotubes nanocomposites as advanced electrode of high-performance aqueous asymmetric supercapacitors", *J. Alloys Compd.*, **885**, p. 160979 (2021).
23. Huang, Y., Peng, J., Luo, J., et al. "Spherical Gr/Si/GO/C composite as high-performance anode material for lithium-ion batteries", *Energy Fuels*, **34**, pp. 7639–7647 (2020).
24. Kalaga, K., Rodrigues, M.T.F., Trask, S.E., et al. "Calendar-life versus cycle-life aging of lithium-ion cells with silicon-graphite composite electrodes", *Electrochim. Acta*, **280**, pp. 221–228 (2018).
25. Astuti, Y., Aprialdi, F., Arnelli, and Haryanto, I. "Synthesis of activated carbon/bismuth oxide composite and its characterization for battery electrode", In *IOP Conference Series: Materials Science and Engineering*, IOP Publishing, **509**, p. 012153 (2019).
26. Gupta, S., Aberg, B., and Carrizosa, S. "Hydrothermal synthesis of vanadium pentoxides-reduced graphene oxide composite electrodes for enhanced electrochemical energy storage", *MRS Adv.*, **1**, pp. 3049–3055 (2016).
27. Wu, C., Shen, L., Huang, Q., et al. "Hydrothermal synthesis and characterization of Bi_2O_3 nanowires", *Mater. Lett.*, **65**, pp. 1134–1136 (2011).
28. Astuti, Y., Musthafa, F., Arnelli, and Nurhasanah, I. "French fries-like bismuth oxide: physicochemical properties, electrical conductivity and photocatalytic activity", *Bulletin of Chemical Reaction Engineering & Catalysis*, **17**(1), pp. 146-156 (2022).
29. Santoso, B. "Sintesis karbon aktif termodifikasi surfaktan HDTMA-Br dengan aktivator h_3po_4 dan radiasi gelombang mikro sebagai adsorben NO_2^-", *Skripsi*, Departemen Kimia, Fakultas Sains dan Matematika, Universitas Diponegoro, Jawa Tengah Indonesia (2019).
30. Di Blasi, C. "Modeling chemical and physical processes of wood and biomass pyrolysis", *Prog. Energy Combust. Sci.*, **34**, pp. 47–90 (2008).
31. Safitri, Z.F., Pangestika, A.W., Fauziah, F., et al. "The influence of activating agents on the performance of rice husk-based carbon for sodium lauryl sulfate and chrome (Cr) metal adsorptions", in *IOP Conference Series: Materials Science and Engineering*, IOP Publishing, **172**, p. 012007 (2017).
32. Yaman, S. "Pyrolysis of biomass to produce fuels and chemical feedstocks", *Energy Convers. Manag.*, **45**, pp. 651–671 (2004).
33. Biswas, B., Pandey, N., Bisht, Y., et al. "Pyrolysis of agricultural biomass residues: Comparative study of corn cob, wheat straw, rice straw and rice husk", *Bioresour. Technol.*, **237**, pp. 57–63 (2017).
34. Muniandy, L., Adam, F., Mohamed, A.R., et al. "The synthesis and characterization of high purity mixed microporous/mesoporous activated carbon from rice husk using chemical activation with NaOH and KOH", *Microporous Mesoporous Mater.*, **197**, pp. 316–323 (2014).
35. Gondal, M., Saleh, T.A., and Drmosh, Q. "Optical properties of bismuth oxide nanoparticles synthesized by pulsed laser ablation in liquids", *Sci. Adv. Mater.*, **4**, pp. 507–510 (2012).
36. Astuti, Y., Amri, D., Widodo, D.S., et al. "Effect of fuels on the physicochemical properties and photocatalytic activity of bismuth oxide, synthesized using solution combustion method", *Int. J. Technol.*, **11**, pp. 26–36 (2020).

37. Astuti, Y., Elesta, P.P., Widodo, D.S., et al. "Hydrazine and urea fueled-solution combustion method for Bi_2O_3 synthesis: characterization of physicochemical properties and photocatalytic activity", *Bull. Chem. React. Eng. Catal.*, **15**, pp. 104–111 (2020).

38. Bandyopadhyay, S., Anirban, S., Sinha, A., et al. "Ionic conductivity of rare earth doped phase stabilized Bi_2O_3: Effect of ionic radius", In *AIP Conference Proceedings*, AIP Publishing LLC, **1832**, p. 110020 (2017).

39. Wazir, A.H., Wazir, I.U., and Wazir, A.M. "Preparation and characterization of rice husk based physical activated carbon", *Energ Source Part A.*, pp. 1–11 (2020).

40. Teo, E.Y.L., Muniandy, L., Ng, E.P., et al. "High surface area activated carbon from rice husk as a high performance supercapacitor electrode", *Electrochim. Acta*, **192**, pp. 110–119 (2016).

41. Zhang, L., Hashimoto, Y., Taishi, T., et al. "Fabrication of flower-shaped Bi_2O_3 superstructure by a facile template-free process", *Appl. Surf. Sci.*, **257**, pp. 6577–6582 (2011).

42. Shen, Y., Li, Y.W., Li, W.M., et al. "Growth of Bi_2O_3 ultrathin films by atomic layer deposition", *J. Phys. Chem. C*, **116**, pp. 3449–3456 (2012).

43. Trivedi, M.K., Tallapragada, R.M., Branton, A., et al. "Evaluation of atomic, physical, and thermal properties of bismuth oxide powder: An impact of biofield energy treatment", *Am. J. Nano Res. Appl.*, **3**, pp. 94–98 (2015).

44. Aflahannisa, A. and Astuti, A. "Sintesis nanokomposit karbon-tio2 sebagai anoda baterai lithium", *J. Fisika Unand*, **5**, pp. 357–363 (2016).

45. Xie, Y., Sohn, S., Wang, M., et al. "Supercluster-coupled crystal growth in metallic glass forming liquids", *Nat. Commun.*, **10**, pp. 1–9 (2019).

46. Sefthymaria, S., Nuryanto, R., and Taslimah, T. "Pengaruh variasi chelating agent terhadap karakteristik produk pada sintesis elektrolit padat $NaMn_{2-x}Mg_xO_4$ dengan metode sol-gel", *J. Kim. Sains Apl.*, **18**, pp. 79–84 (2015).

47. Yang, Z., Shen, J., and Archer, L.A. "An in situ method of creating metal oxide-carbon composites and their application as anode materials for lithium-ion batteries", *J. Mater. Chem.*, **21**, pp. 11092–11097 (2011).

48. Berger, L.I., *Semiconductor Materials*, CRC Press (1996).

49. Thommes, M., Kaneko, K., Neimark, A.V., et al. "Physisorption of gases, with special reference to the evaluation of surface area and pore size distribution (IUPAC Technical Report)", *Pure Appl. Chem.*, **87**, pp. 1051–1069 (2015).

50. Subhan, A. "Fabrikasi dan karakterisasi $Li_4Ti_5O_{12}$ untuk bahan anoda Baterai Lithium Keramik: Sinthesis and characterization of $Li_4Ti_5O_{12}$ as anode material for lithium ceramic battery", Thesis, Program Studi Teknik Metalurgi dan Material, Universitas Indonesia, Jakarta Indonesia (2011).

51. Cai, J., Wei, W., Hu, X., et al. "Electrical conductivity models in saturated porous media: A review", *Earth Sci. Rev.*, **171**, pp. 419–433 (2017).

52. Kultayeva, S., Ha, J.H., Malik, R., et al. "Effects of porosity on electrical and thermal conductivities of porous SiC ceramics", *J. Eur. Ceram. Soc.*, **40**, pp. 996–1004 (2020).

Biographies

Yayuk Astuti is a lecturer in Chemistry at Faculty of Sciences and Mathematics, Universitas Diponegoro, Indonesia. She obtained her BSc degree in Chemistry at the Department of Chemistry, FMIPA Universitas Diponegoro, Indonesia in October 2005. In less than a year of graduation, Yayuk Astuti was accepted as a lecturer at the same university. PhD degree was obtained through an accelerated program at Newcastle University, UK in early 2014 (Master leading to PhD). Currently, her research concern is material chemistry, especially synthesis, modification, characterization, and application. Some of the materials that have been developed are carbon, nanodiamond, and bismuth oxide for adsorbents, battery electrodes, drug carriers, and photocatalysts.

Roshana Mei was an undergraduate student at Fakultas Sains dan Matematika, Universitas Diponegoro, Indonesia in 2016. She received her BSc degree in Chemistry in 2020. Her research project was synthesis of bismuth oxide/activated carbon composite for battery anode.

Adi Darmawan is a lecturer at the Chemistry Department, Faculty of Sciences and Mathematics, Universitas Diponegoro, Indonesia. He received his BSc degree at the same university that worked in 1996 and his MS degree was received from the Department of Chemistry, Gadjah Mada University, Indonesia in 2003. In 2014, he received his PhD degree from School of Chemical Engineering, University of Queensland, Australia. His research interest is inorganic materials, especially in silica and carbon for membrane separation.

Arnelli has been a chemistry lecturer at Fakultas Sains dan Matematika, Universitas Diponegoro, Indonesia since 1989. She studied undergraduate at Andalas University from 1979 to 1986 in Pure Chemistry and obtained MSc degree at Bandung Institute of Technology (ITB) in 1989 in the same field, especially chemical physics. Her research interests are surfactant and its

application, activated carbon, and its modification for adsorbent.

Hendri Widiyandari has been a lecturer at the Physics Department Sebelas Maret University, Indonesia since 2018. Before that, she had been a lecturer at the Department of Physics, Diponegoro University, Indonesia from 1999 until 2017. She received her PhD degree in Chemical Engineering from Hiroshima University, Japan. Her research interest is in the synthesis and characterization of functional materials for energy storage and conversion. One of the research interests is the development of active materials for Li-ion batteries.